

Influence of Collective Surface Motion on the Threshold Behaviour of Nuclear Fusion

W. Reisdorf, F.P. Heßberger, K.D. Hildenbrand, S. Hofmann, G. Münzenberg, J.H.R. Schneider,  
W.F.W. Schneider, K. Sümmerer, G. Wirth  
GSI Darmstadt  
J.V. Kratz, K. Schlitt  
Institut für Kernchemie, Universität Mainz

Recently measured <sup>1</sup> fusion excitation functions that extend from the  $\mu\text{b}$  level up to several 100 mb have been used to test a potential model for fusion that includes a fluctuation of the barrier with an amplitude that can be related to known collective nuclear properties.

Typical data, shown in Fig. 1, can be parametrized over the full energy range (full curves) by two parameters only: an average fusion barrier  $V_B$  and a standard fluctuation width  $\sigma(V_B)$  of the barrier. Table 1 shows a list of parameter values found for a number of systems <sup>1,2</sup>.

In the fitting procedure we use a nucleus-nucleus potential of the form  $V(s) = V_n R_{12} \exp(-s/d)$  with  $s=r-(R_1+R_2)$  and  $R_{12} = R_1 R_2 / (R_1 + R_2)$ ,  $d = 0.75$  fm. The central radii are deduced from published RMS radii,  $V_n$  is adjusted to the data and determines the average fusion barrier. A Gaussian distribution of fusion barriers is generated by assuming, and adjusting, a Gaussian distribution  $\sigma(R_1+R_2)$  (Col. 3 of Table 1) of the sum of radii and calculating the fusion excitation functions by a weighted superposition. Sub-barrier penetration was calculated by a WKB method. The barrier fluctuation can be interpreted as a "vibrational" fluctuation of the surface-to-surface distance originating from the collective vibrational motion of the surfaces<sup>3</sup>. It is then directly correlated to deformation lengths  $BR$  determined in inelastic scattering - such as  $(\alpha, \alpha')$  - experiments. By an incoherent addition of contributions from low-lying ( $< 3$  MeV) octupole and quadrupole states in both projectile and target nuclei we can estimate the sum-of-radii fluctuation  $\sigma_{ZP}(R_1+R_2)$  expected from zero-point surface motion. This is shown in Table 1 and is consistent in detail with the values deduced from the fusion data. The orientational part of the fluctuation (<sup>154</sup>Sm) is not included in Table 1. In the figure we illustrate for <sup>40</sup>Ar+<sup>122</sup>Sn how the introduction of a barrier fluctuation phenomenon influences the general behaviour of the excitation function. If we first shut off the tunnelling process in the calculation, we obtain the left dotted curve which fails to describe the energy range marked "T" (for tunnelling) below the mb level, but describes well the range above it. If we also shut off the fluctuation (right dotted curve), we can still describe the data in the "classical" range marked "C". The amplitude of the barrier fluctuation is determined rather well from the intermediate range "F", once  $V_B$  (or equivalently,  $V_n$ )

has been fixed by the data in range C. For <sup>40</sup>Ar+<sup>154</sup>Sm we have also plotted a curve showing separately the effect of the "orientational" fluctuations, i.e. the known static deformation (dash-dotted curve). The dashed curves represent the conventional calculation without static deformation and vibrational fluctuation.

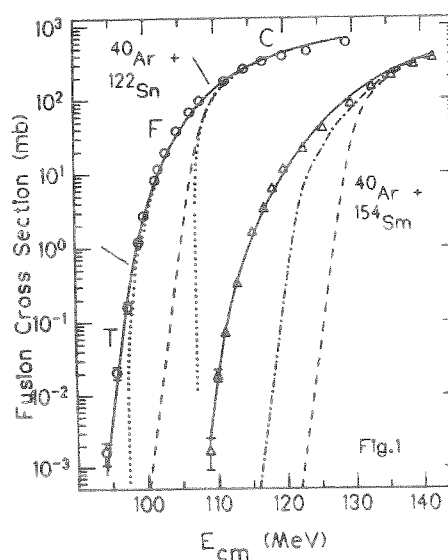
Table 1: Parameters deduced from fusion excitation functions <sup>1,2</sup>.

System	$V_B$ (MeV)	$\sigma(V_B)$ %	$\sigma(R_1+R_2)$ %	$\sigma_{ZP}(R_1+R_2)$ %
<sup>40</sup> Ar+ <sup>112</sup> Sn	109.1	4.0	4.7	4.85
<sup>40</sup> Ar+ <sup>116</sup> Sn	108.3	3.9	4.6	4.95
<sup>40</sup> Ar+ <sup>122</sup> Sn	107.2	3.9	4.5	4.85
<sup>40</sup> Ar+ <sup>144</sup> Sm	130.2	3.4	3.9	4.4
<sup>40</sup> Ar+ <sup>148</sup> Sm	129.4	4.3	4.9	5.0
<sup>40</sup> Ar+ <sup>154</sup> Sm	129.3	3.75	4.2	3.8
<sup>16</sup> O+ <sup>148</sup> Sm	60.25	2.9	3.6	4.5
<sup>16</sup> O+ <sup>154</sup> Sm	59.9	2.2	2.8	2.3

<sup>1</sup>W. Reisdorf et al., Phys. Rev. Lett. 49, 1811 (1982)

<sup>2</sup>R.G. Stokstad et al., Phys. Rev. Lett. 47, 465 (1978)

<sup>3</sup>H. Esbensen, Nucl. Phys. 1352, 147 (1981).



Evaporation Residue Cross Sections in the Fusion of  $^{86}\text{Kr}$  with Ge, Mo, and Ru Isotopes

W. Reisdorf, F.P. Heßberger, K.D. Hildenbrand, S. Hofmann, G. Müzenberg, J.H.R. Schneider,  
W.F.W. Schneider, K. Sümmerer, G. Wirth  
GSI Darmstadt  
J.V. Kratz, K. Schlitt  
Institut für Kernchemie, Universität Mainz

The analysis of evaporation residue data obtained by combining activation methods with the use of the velocity filter SHIP<sup>1</sup> has been continued with special emphasis on  $^{86}\text{Kr}$  induced fusion with  $^{70,76}\text{Ge}$ ,  $^{92,100}\text{Mo}$ , and  $^{99,102,104}\text{Ru}$ . On the low-energy side the data extend down to about 10  $\mu\text{b}$ . Three features of the data are illustrated in Figs. 1 and 2.

1) The saturation of the evaporation residue cross sections at high angular momenta, presumably by fission, shows clear-cut isotopic trends. This is stressed by plotting the quantity  $l_{\text{max}} = (\sigma_{\text{ER}}/\pi\lambda^2)^{1/2}$  vs.  $E_{\text{cm}}$ , where  $\sigma_{\text{ER}}$  is the evaporation residue cross section,  $\lambda$  the de Broglie wavelength and  $E_{\text{cm}}$  the center-of-mass energy (Fig. 1). Whereas the system  $^{86}\text{Kr} + ^{100}\text{Mo} + ^{186}\text{Pt}$  saturates at  $l_{\text{max}} = 35 \pm 2$ , the system  $^{86}\text{Kr} + ^{92}\text{Mo} + ^{178}\text{Pt}$  has  $l_{\text{max}} = 21 \pm 1$ . Similar trends were observed for the Ru targets (leading to Hg compound nuclei). We hope that the data will allow to determine isotopic trends in fissionability and provide long needed information on the stability of excited proton rich nuclei against fission.

2) From a comparison of the slopes of the excitation functions, cf.  $^{100}\text{Mo}$  vs.  $^{92}\text{Mo}$  in Fig. 1, it is again<sup>1</sup> apparent that the surface properties ( $^{92}\text{Mo}$  has a closed neutron shell) influence the variation of the fusion cross section below the average fusion barrier.

3) Some of the new data lead to the same compound nuclei as the  $^{40}\text{Ar}$  induced fusion data obtained earlier<sup>1</sup>. This allows to study the entrance channel influence on the fusion process. In Fig. 2 we have plotted  $l_{\text{max}}$  vs.  $E_{\text{cm}}$  for  $^{40}\text{Ar} + ^{148}\text{Sm}$  and  $^{86}\text{Kr} + ^{102}\text{Ru}$  leading both to the compound nucleus  $^{188}\text{Hg}$ . The  $^{86}\text{Kr} + ^{102}\text{Ru}$  data have been rescaled along the  $E_{\text{cm}}$  axis using the proximity scaling<sup>2</sup>. Whereas this leads to overlapping curves (not shown) for systems involving Er ( $Z=68$ ) compound nuclei, this is not the case in Fig. 2. Notice that the saturating angular momenta agree approximately as expected from a compound picture. Two possible interpretations for the relative "hindrance" of the  $^{86}\text{Kr} + ^{102}\text{Ru}$  Ru data will be further investigated in the future a) a failure of the proximity scaling b) a possible hindrance to fusion for heavier and symmetric systems. In terms of the barrier fluctuation introduced earlier<sup>1</sup> it could mean that for these systems the full fluctuation width of the zero-point surface- to-surface vibrations is no longer to be found in the fusion channel, but possibly in transfer channels.

<sup>1</sup>W. Reisdorf et al., Phys. Rev. Lett. 49, 1811 (1982)

<sup>2</sup>J. Blocki et al., Ann. Phys. (N.Y.) 105, 427 (1977)

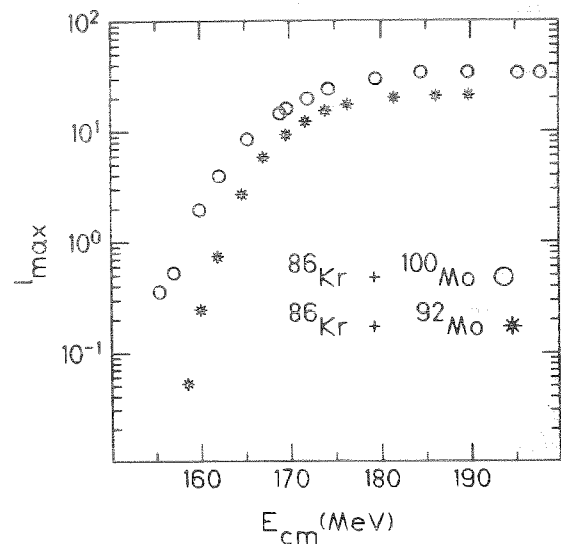


Fig. 1 Excitation functions for  $l_{\text{max}} = (\sigma_{\text{ER}}/\pi\lambda^2)^{1/2}$

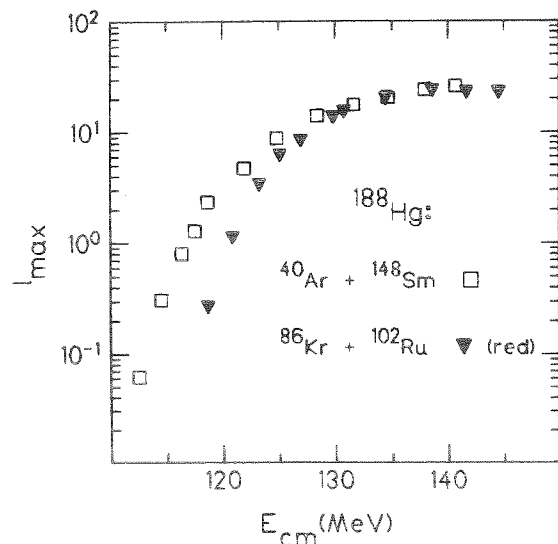


Fig. 2 Same as Fig. 1. The  $^{86}\text{Kr} + ^{102}\text{Ru}$  data have been rescaled along the  $E_{\text{cm}}$  axis using the proximity scaling.

Capture-Fission in the Reaction  $^{76}\text{Ge} + ^{170}\text{Er}$

K.Lützenkirchen and J.V.Kratz, Institut für Kernchemie, Universität Mainz

W.Brüchle, H.Gäggeler, K.Sümmerer and G.Wirth, GSI Darmstadt

Various attempts have recently been made to investigate the dynamical limitations of the fusion of heavy nuclei. A particular class of experiments was the production of  $^{246}\text{Fm}$  compound nuclei /1/ through a variety of entrance channels, one of which was  $^{76}\text{Ge} + ^{170}\text{Er}$ .

The fusion cross section  $\sigma_f$  was usually determined by measuring the spontaneous fission decay of the  $(\text{HI}, 2n)$   $^{244}\text{Fm}$  evaporation residues. In the case considered here, we found the fusion process to be considerably hindered. To check this result, we decided to measure the fission cross section of the hypothetical compound nucleus  $^{246}\text{Fm}^*$ .

The respective irradiation was performed at the UNILAC accelerator, using a  $^{76}\text{Ge}$ -beam ( $E=5.18 \text{ MeV/A}$ ), a thick  $^{170}\text{Er}$ -target ( $5.06 \text{ mg/cm}^2$ ) and a total of  $3.4 \times 10^{15}$  incident particles. The products were caught in an aluminum foil stack. Cross sections for individual isotopes were determined via their characteristic  $\gamma$ -ray transitions.

Fig.1 depicts the cross sections  $\sigma_c$  for symmetric fragmentation of one of the catcher foils. A gaussian distribution with  $\text{FWHM}=5.0 \text{ amu}$  is well suited to represent the data. The experimentally deduced maxima of the distribution  $\langle A \rangle_Z$  for given  $Z$  are in accord with calculations based upon minimizing the potential energy and correcting for neutron evaporation. Considering the  $Z$ -dependence of  $\langle A \rangle_Z$  we were able to construct the mass distribution for each catcher foil and the total element distribution (Fig.2).

Although an excitation energy range of 35 MeV through 65 MeV was covered, we obtained a double humped distribution of fission products. The peak-to-valley ratio turns out to be 2:1 and the average charge asymmetry is about 1:1.3. These facts indicate that the starting point for fission might have been the compound nucleus  $^{246}\text{Fm}^*$ . Nevertheless, processes leading to complete mass equilibration via non-compound reactions (fast-fission) cannot be excluded with certainty.

The thick target cross section deduced from fig.2 is  $\sigma_c = 94_{-33}^{+44} \text{ mb}$ . This result is suitably explained within Swiatecki's Extra-Push model /2/, when we

assume an extra-push of  $E_x = 10 \pm 5 \text{ MeV}$  over the static fusion barrier  $B$  ( $B = 0.96 \times B_{\text{prox}} = 227.1 \text{ MeV}$ ).

Within error limits this value is in agreement with the one deduced from the evaporation residue measurement, which was  $E_x = 12_{-5}^{+\infty} \text{ MeV}$ .

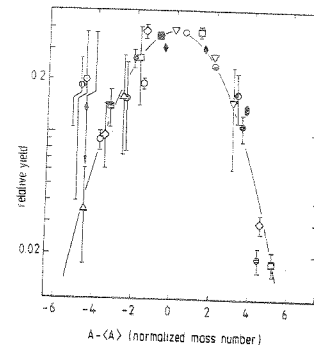


Fig.1. Yields corrected for precursor decay at constant  $Z$  versus mass number  $A$  normalized with respect to the centroid  $\langle A \rangle_Z$  and the element yield  $P(Z)$  of each isotope distribution.

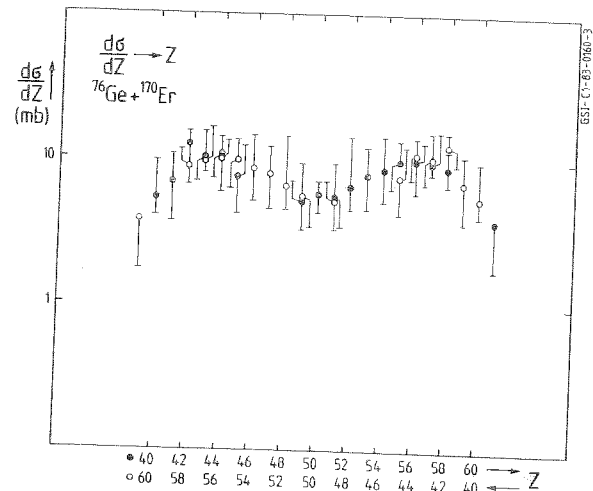
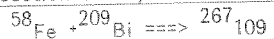


Fig.2. Element distribution for symmetric fragmentation ( $\bullet$ ) and distribution reflected at  $Z=50$  ( $\circ$ ). Cross sections for the elements  $Z=39, 46, 47, 48, 59, 60$ , for which only lower limits exist, are not shown. An estimated portion of the cross section contributed by the deep-inelastic products was subtracted from  $Z=40-43, 61$ .

/1/ H.Gäggeler et al., Proc.Int. Workshop on Gross Properties of Nuclei and Nuclear Excitations X, Hirschegg 1982,40 (1982)

/2/ W.J.Swiatecki, Nucl.Phys. A376 (1982) 275

An Estimate of the Cross-section for symmetric Fragmentation in the Reaction



K.Lützenkirchen and J.V.Kratz, Institut für Kernchemie, Universität Mainz

W.Brüchle, H.Gäggeler, K.Sümmerer and G.Wirth, GSI Darmstadt

During the  ${}^{58}\text{Fe} + {}^{209}\text{Bi}$ -experiment, performed at the velocity filter SHIP /1/, we installed an aluminum foil behind the target, suited to catch the fission products. The catcher-foil arrangement covered the angle  $\Delta\Omega = 1.6 \pm 0.2$  sr and allowed the evaporation residues to pass through a hole around  $0^\circ$ . At the two laboratory energies 4.95 MeV/A and 5.15 MeV/A  $2 \times 10^{17}$  and  $3 \times 10^{17}$  particles were accumulated on the target, respectively. An iodine fraction was chemically separated from the rest of the products and was subjected to  $\gamma$ -ray measurements.

Iodine ( $Z=53$ ) represents the products emerging from symmetric fragmentation. At 4.95 MeV/A we could not detect any iodine isotopes (cross-section limit  $\leq 0.3$   $\mu\text{b}$ ), whereas at 5.15 MeV/A we identified the isotopes  ${}^{123}\text{I}$ ,  ${}^{124}\text{I}$ ,  ${}^{126}\text{I}$  and  ${}^{130}\text{I}$  (Fig.1). Integration over the resulting gaussian distribution, followed by a second integration over the total  $Z$ -distribution, had us arrive at a cross-section for symmetric fragmentation of  $\sigma = 3.1 \pm 1.3$  mb at 5.15 MeV/A. The  $Z$ -distribution was assumed to be gaussian also with an estimated FWHM of 21  $Z$ -units./2/

For 4.95 MeV/A we obtained an upper limit for the cross-section of  $\sigma \leq 0.3^{+0.7}_{-0.2}$  mb. The magnitude of both cross-sections gives good reason to suspect that both energies were close to or below the fusion barrier. Using the equation

$$\sigma_f = (\hbar^2 \omega^2 / 2E) \times \ln(1 + \exp(2\pi(E-B)/\hbar\omega)),$$

which represents the fusion cross-section below the barrier, and the parameters  $r_f = 12.3$  fm,  $\hbar\omega = 8^{+12}_{-5}$  MeV,  $E = 233.8$  MeV, one deducts a barrier of  $B = 236.5^{+7}_{-2}$  MeV.

This result implies an extra-push of  $11.7^{+7}_{-2}$  MeV ( $0.96 \times B_{\text{prox}} = 224.8$  MeV), a value which is consistent with other results concerning the dynamical limitations of the fusion process. (Fig.2 at  $x_{\text{eff}} \approx 0.8$ )

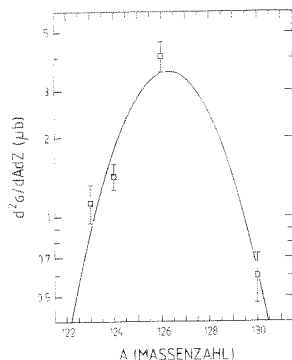


Fig.1. Mass distribution of the iodine isotopes from symmetric fragmentation in the reaction  ${}^{58}\text{Fe} + {}^{209}\text{Bi}$ . FWHM equals 4.7, the most probable mass number is  $\langle A \rangle_Z = 126$ .

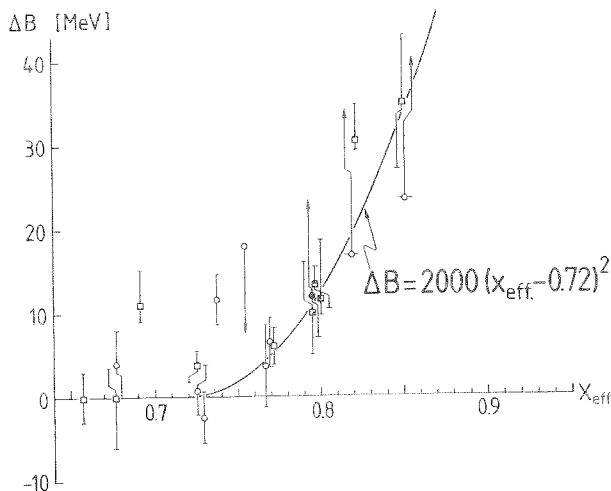


Fig.2. Differences between experimental and calculated fusion barriers ( $0.96 \times B_{\text{prox}}$ ) as a function of  $x_{\text{eff}}$  /3,4,5,6/.

${}^{58}\text{Fe} + {}^{209}\text{Bi}$ ,  ${}^{58}\text{Fe} + {}^{208}\text{Pb}$ ,  ${}^{76}\text{Ge} + {}^{170}\text{Er}$  (sym. fragmentation),  ${}^{76}\text{Ge} + {}^{170}\text{Er}$  (evaporation residues).

- /1/ G.Münzenberg et al., Z.Physik A,309,89 (1982)
- /2/ C.-C.Sahm et al., Z.Physik A,297,241 (1980)
- /3/ H.Gäggeler et al., Proc.Int. Workshop on Gross Properties of Nuclei and Nuclear Excitations X, Hirschegg 1982,40 (1982)
- /4/ K.-H.Schmidt et al., Z.Physik,A301,21 (1981)
- /5/ G.Münzenberg et al., Z.Physik,A302,7 (1981)
- /6/ R.Bock et al., Nucl.Phys.A388,334 (1982)

Sub-Coulomb Transfer in Collisions of  $^{239}\text{U}$  with  $^{238}\text{U}$  B

G. Wirth, W. Brüche, Fan Wo, H. Gaeggeler, K. Schlitt, K. Sümmerer  
GSI Darmstadt

J.V. Kratz, M. Lerch, N. Trautmann Institut für Kernchemie, Universität Mainz

Structures in the positron spectra observed in U-U collisions<sup>1</sup> are discussed as experimental evidence for the process of spontaneous positron production. However, a nuclear background may arise from internal electron-positron pair creation during the decay of excited nuclei, which was determined from the corresponding  $\gamma$ -ray spectrum applying semi-empirical internal pair-conversion coefficients measured in low Z systems. This procedure assumes for different reactions similar multiplicities and may be problematic for  $\gamma$ -transitions from the deexcitation of quasielastic transfer products. Cross sections for quasielastic transfer are known to have a strong dependence on the incident energy of the projectile near the barrier<sup>2</sup>. EO-transitions are completely neglected. Therefore we have measured cross sections radiochemically for several xn, 1pxn and 2pxn transfer channels in the system U + U at incident lab-energies of 5.5, 5.8, 5.9 and 6.1 MeV/u. The targets consisted of 380  $\mu\text{g}/\text{cm}^2$  Uranium covered with Titanium of 20  $\mu\text{g}/\text{cm}^2$  respectively 120  $\mu\text{g}/\text{cm}^2$  on the side opposite to the beam. Catcher foils were placed in the whole angular range from the target to  $45^\circ$ . Following a bombardment the targets and catcher foils were removed and chemically separated. Through  $\gamma$ -ray counting the absolute decay rates and from that cross sections for individual transfer products were determined. Data analysis is still in progress. Some preliminary cross sections are

5.9 MeV/u:	$^{239}\text{U}$	(1n)	$95 \pm 10$ mb
	$^{240}\text{U}$	(2n)	$5 \pm 1$ mb
	$^{238}\text{Np}$	(1p1n)	$0.9 \pm 0.15$ mb
5.8 MeV/u:	$^{239}\text{U}$	(1n)	$61 \pm 12$ mb
	$^{237}\text{Pa}$	(1p)	$2.6 \pm 0.5$ mb
5.5 MeV/u:	$^{239}\text{U}$	(1n)	$23 \pm 3$ mb
	$^{237}\text{Pa}$	(1p)	$0.45 \pm 0.1$ mb

The measurement of the excitation function or angular distributions for  $^{239}\text{U}$  (one neutron transfer) at energies below the barrier should give totally equivalent information if the transfer proceeds under semiclassical conditions and the slopes of the angular distributions and of the excitation function should then be determined only by the neutron binding energy in  $^{238}\text{U}$ <sup>3</sup>. The peak structure in the positron spectra is most pronounced at ion scattering angles  $\theta_{\text{lab}} = 45^\circ$  and nuclear collisions with a relatively long reaction time as indicated by the width of the positron line<sup>1</sup> could show up in deviations from the expected semiclassical behaviour for quasielastic nucleon transfer assuming pure

Rutherford scattering. Therefore we have measured the angular distributions for one neutron transfer at energies near the barrier and well below it and the excitation function for the formation of  $^{239}\text{U}$  down to 73 % of the "spherical" Coulomb barrier using an interaction radius  $R_{\text{int}} = 1.16(A_1^{1/3} + A_2^{1/3} + 2)$  fm. Still at 73 % of the barrier there is a cross section of 0.16 mb for the formation of  $^{239}\text{U}$ . The data points of the excitation function plotted in fig. 1 are expected to fall on a straight line with a slope shown by the solid line. Fig. 2 shows the angular distribution of  $^{239}\text{U}$  at  $E_{\text{lab}} = 5.7$  MeV/u, expected to be backward-peaked. A decrease of the differential cross section at the very backward angles is observed and is also seen at beam energies of 5.9, 5.4 and 5.1 MeV/u. It has to be checked, whether this can be accounted for by Coulomb excitation along the trajectories before and after the neutron transfer and subsequent fission.

1. E. Berdermann et al., GSI Scientific Report 1981, GSI 82-1 (1982) 138  
H. Bokemeyer et al., GSI Scientific Report 1981, GSI 82-1 (1982) 139
2. G. Franz et al., Z. Physik A 291, 167 (1979)
3. W. von Oertzen in Nuclear Spectroscopy and Reactions Vol.B ed. J. Cerny (Academic Press) p. 279

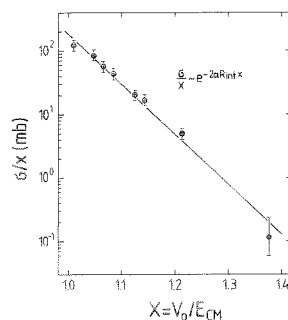


Fig.1:  
Excitation function for the formation of  $^{239}\text{U}$  in the U+U reaction. The solid line has the semi-classically expected slope whereas the absolute scaling was fitted to the experimental points.  
 $V_0 = e^2 Z_1 Z_2 / R_{\text{int}}$   
 $R_{\text{int}} = 1.16(A_1^{1/3} + A_2^{1/3} + 2)$  fm;  
 $\alpha = (2mB_n / \hbar^2)^{1/2}$

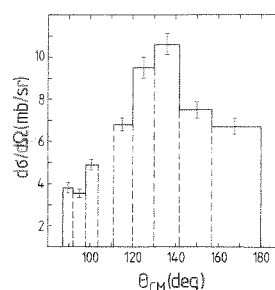


Fig.2:  
Angular distribution of  $^{239}\text{U}$  from U-U collisions at  $E_{\text{lab}} = 5.7$  MeV/u.

Heavy Actinide Products from Reactions of  $^{18}\text{O}$  and  $^{22}\text{Ne}$  with  $^{254}\text{Es}$ 

M. Schädel<sup>+</sup>, R.W. Loughheed<sup>\*</sup>, J.H. Landrum<sup>\*</sup>, J.F. Wild<sup>\*</sup>, R.J. Dougan<sup>\*</sup>,  
A.D. Hoover<sup>\*</sup>, E.K. Hulet<sup>\*</sup>, A. Ghiorso<sup>‡</sup>, K.J. Moody<sup>‡</sup>, and G.T. Seaborg<sup>‡</sup>

<sup>+</sup> GSI Darmstadt, <sup>\*</sup> LLNL, Livermore CA, <sup>‡</sup> LBL, Berkeley CA

We carried out a series of bombardments using  $^{254}\text{Es}$  as the target nuclide and  $^{18}\text{O}$  and  $^{22}\text{Ne}$  as the projectile. In our experiments we used chemical techniques to separate element fractions from a catcher foil after end of bombardment, and measured these fractions to obtain  $\alpha$ -energy spectra and count SF events.

Cross sections for the Fm and Md isotopes and  $^{259}\text{No}$  from the reactions of 121-MeV  $^{22}\text{Ne}$ , 125-MeV  $^{22}\text{Ne}$  and 98-MeV  $^{18}\text{O}$  with  $^{254}\text{Es}$  are shown in Figure 1. Fermium formation cross sections from 97-MeV  $^{18}\text{O} + ^{248}\text{Cm}$  [1] are shown for comparison.

For the  $^{22}\text{Ne} + ^{254}\text{Es}$  reaction, we observed only a very slight increase in cross sections with increasing energy. The shape of the isotopic distributions shown do not shift significantly. To determine the most probable mass ( $A_p$ ), we fitted a gaussian curve to the data and held  $\sigma = .977u$  (FWHM = 2.3u) fixed. For the Fm isotopes, we found  $A_p = 254.5$ , and  $A_p(\text{Md}) = 256.0$ .

More neutron rich products were observed in the  $^{18}\text{O} + ^{254}\text{Es}$  reaction at 98-MeV incident energy than were found at 121-MeV  $^{22}\text{Ne}$ .  $A_p$ -values of 255.5 for Fm and 257.1 for Md were determined. This makes the  $^{18}\text{O}$  the most favourable projectile for the production of neutron rich heavy actinides when compared to  $^{22}\text{Ne}$ . The Fm cross section is enhanced by a factor of  $10^3$  and the Md cross section by more than  $10^4$  when the yields from a  $^{254}\text{Es}$  target are compared with a  $^{248}\text{Cm}$  target [1].

In the reactions with  $^{18}\text{O}$  as a projectile on  $^{248}\text{Cm}$  and  $^{254}\text{Es}$  targets, we were able to extrapolate ( $E_s^{254}, x$ ) cross sections from cross sections measured [1] with a  $^{248}\text{Cm}$  target assuming (i) an equal transfer probability for a given number of protons ( $\Delta Z$ ) and neutrons ( $\Delta N$ ), and (ii) no significant shift of the primary fragment distribution by neutron evaporation or fission. This is possible only in these light ion reactions at the barrier where the excitation energies are less than the neutron separation energies and fission barriers, whereas, there are large differences in cross sections for products with the same number of transferred nucleons ( $\Delta Z, \Delta N$ ) in reactions with  $^{238}\text{U}$  projectiles on  $^{238}\text{U}$  and  $^{248}\text{Cm}$  targets [2]. Isotope cross sections are in good agreement for two proton transfer products on  $^{248}\text{Cm}$  and  $^{254}\text{Es}$  as a target and  $^{18}\text{O}$  as a projectile, while small differences in cross section for  $^{22}\text{Ne}$  may be due to a slightly higher projectile energy with the  $^{254}\text{Es}$  target. We used these isotope

distributions, and a similar method for three and four proton transfer, to estimate cross section for unknown, neutron-rich heavy actinides. The results are given in Table 1. It is important to note that these estimates still contain large uncertainties because we are not yet able to predict the exact  $A_p$  position of the isotope distribution. However, it is fascinating to see that exotic nuclei like  $^{261}\text{Md}$ ,  $^{261}\text{No}$  or  $^{262}\text{Lr}$  should be accessible in reactions of  $^{18}\text{O}$  with  $^{254}\text{Es}$ .

[1] D. Lee et al., Phys. Rev. C25, 286 (1982)

[2] M. Schädel et al., Phys. Rev. Lett. 48, 852 (1982)

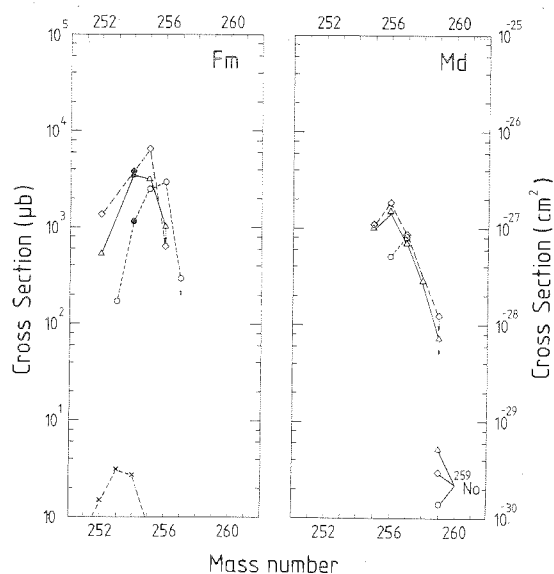


Figure 1: Cross sections for  $^{259}\text{No}$  and Fm and Md isotopes in the reaction 121-MeV  $^{22}\text{Ne} + ^{254}\text{Es}$  (symbol =  $\Delta$ ), 125-MeV  $^{22}\text{Ne} + ^{254}\text{Es}$  (symbol =  $\diamond$ ) and 98-MeV  $^{18}\text{O} + ^{254}\text{Es}$  (symbol =  $\circ$ ). Cross sections for Fm isotopes in the reaction 97-MeV  $^{18}\text{O} + ^{248}\text{Cm}$  from Ref. 1 (symbol =  $+$ ) are shown for comparison. Open symbols are independent, full symbols are cumulative yields, arrows indicate that these cross sections are upper limits only. The curves are drawn to connect the data point.

TABLE 1: Estimated transfer cross section in  $\mu\text{b}$  for unknown neutron-rich actinides

Reaction	Transfer cross section [ $\mu\text{b}$ ]					
	$^{260}\text{Md}$	$^{261}\text{Md}$	$^{260}\text{No}$	$^{261}\text{No}$	$^{261}\text{Lr}$	$^{262}\text{Lr}$
$^{18}\text{O} + ^{254}\text{Es}$	9.	.3	5.	.2	.7	.3
$^{22}\text{Ne} + ^{254}\text{Es}$	.3	$\leq .05$	2.	.1	1.	.2

A New 105-ms Spontaneous Fission Activity Produced in the Reaction  $^{180}\text{O}$  with  $^{254}\text{Es}$

L. P. Somerville<sup>ε</sup>, M. J. Nurmia<sup>ε</sup>, M. Schädel<sup>+\*</sup>, A. Ghiorso<sup>ε</sup>, J. M. Nitschke<sup>ε</sup>,  
R. W. Lougheed<sup>\*</sup>, J. H. Landrum<sup>\*</sup>, E. K. Hulet<sup>\*</sup>

<sup>ε</sup>LBL, Berkeley CA, <sup>+</sup>GSI Darmstadt, <sup>\*</sup>LLNL Livermore CA

Measurements of isotope cross sections and estimate for the production of yet unknown isotopes in the reaction  $^{180}\text{O} + ^{254}\text{Es}$  have shown that this reaction is exceptionally well suited to investigate the frontier of very heavy neutron-rich nuclei [1].

To search for short-lived spontaneous fission (SF) emitters with half-lives between 10 ms and 5 seconds we used a recoil tape-transport system [2,3]. All heavy recoils from the reaction 99-MeV  $^{180}\text{O} + ^{254}\text{Es}$  were implanted into a moving stainless steel tape that transported the activity along a series of mica SF-track detectors. Consistent half-lives and cross sections for a new SF-activity were measured from separate experiments with tape speeds of  $0.2\text{ ms}^{-1}$  and  $0.9\text{ ms}^{-1}$ , respectively. The weighed average half-life from both experiments is  $(105 \pm 7)\text{ms}$ , and the cross section  $1.1\text{ }\mu\text{b}$ . The decay curve from one of the experiments ( $0.2\text{ ms}^{-1}$ ) is shown in Figure 1. The long-lived background that is observed in Figure 1 is due primarily to EC-decay of  $^{256}\text{Md}$  into the SF-isotope  $^{256}\text{Fm}$  also produced in the bombardment [1].

We do not yet know the identity of this 105-ms SF emitter. But the  $1\text{ }\mu\text{b}$  cross section for the reaction 99-MeV  $^{180}\text{O} + ^{254}\text{Es}$  is consistent with the cross section estimates for  $^{261}\text{Md}$  ( $3\text{ }\mu\text{b}$ ),  $^{260,261}\text{No}$  ( $5, .2\text{ }\mu\text{b}$ ) or  $^{261,262}\text{Lr}$  ( $.7, .3\text{ }\mu\text{b}$ ) [1], extrapolated from similar transfer channels in the reaction  $^{180}\text{O}$  with  $^{248}\text{Cm}$ . A measured cross-section upper limit of  $80\text{ nb}$  in the reaction  $125\text{-MeV } ^{22}\text{Ne} + ^{254}\text{Es}$  is, however, much lower than expected for  $^{260}\text{No}$  and  $^{261}\text{Lr}$ , but would be consistent with estimates for  $^{261}\text{Md}$ . Bearing in mind the large uncertainties in the estimated cross sections, it is premature for an assignment to one specific neutron rich isotopes of elements 101 through 103. An assignment of the 105-ms activity to an isotopes of element  $Z=104$  seem to be not possible, as none of the  $Z=104$  isotopes is expected to be produced with cross sections larger than  $50\text{ nb}$  in the reaction of  $^{180}\text{O}$  or  $^{22}\text{Ne}$  with  $^{254}\text{Es}$ .

A 105-ms SF half-life for a new, neutron-rich isotope between  $^{101}\text{Md}$  and  $^{103}\text{Lr}$  creates an interesting problem as theoretical estimates for SF half-lives [4,5,6] differ strongly in this very neutron-rich region. For lack of experimental data it is an open question whether the

new systematic of half-lives which was observed for isotopes of element 104 [7] can already be observed for neutron-rich  $^{102}\text{No}$  isotopes. An assignment of the 105-ms isotope will be very important and future experiments can yield more information. With a half-life of 105 ms and a relatively high cross section of  $1.1\text{ }\mu\text{b}$  it will also be possible to study in detail the decay of this isotope, e.g. total kinetic energy and mass division of fission fragments.

- [1] M. Schädel et al., contribution to this report, and Proc. Int. Workshop on Gross Properties of Nuclei and Nuclear Excitations XI, Hirschegg, 1983, in press.
- [2] J. M. Nitschke et al., Lawrence Berkeley Laboratory Annual Report, 1977-78, LBL-8151, p. 84, 1979.
- [3] L. P. Somerville, Ph. D. thesis, Lawrence Berkeley Laboratory Report LBL-15027, 1982.
- [4] A. Baran et al., Nucl. Phys. **A361**, 83 (1981)
- [5] J. Randrup et al., Phys. Rev. **C13**, 229 (1976)
- [6] V. A. Druin et al., Sov. J. Nucl. Phys. **29**, 591 (1979)
- [7] Yu. Ts. Oganessian et al., Pisma Yh. Eksp. Teor. Fiz. **20**, 580 (1974) [JETP Lett. **20**, 265 (1974)]

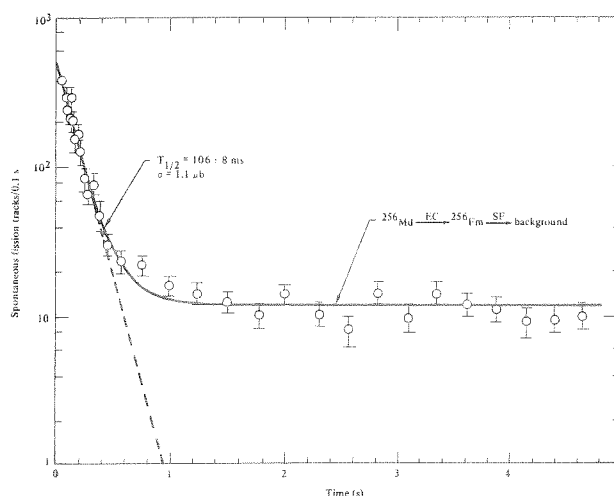


Figure 1:  
Decay curve of a new 105 ms SF-activity produced in the 99-MeV  $^{180}\text{O} + ^{254}\text{Es}$  reaction. The result shown is from one experiment with a tape-speed of  $0.2\text{ m/s}$ .

Recent Searches for Long-lived Superheavy Elements from the  $^{48}\text{Ca} + ^{248}\text{Cm}$  Reaction

B

H. Gäggeler, W. Bröchle, M. Brügger, M. Schädel, K. Sümmerer, G. Wirth

GSI Darmstadt

A. Ghiorso, K.E. Gregorich, D. Lee, K.J. Moody, G.T. Seaborg, R.B. Welch, P. Wilmarth

Lawrence Berkeley Laboratory

G. Herrmann, J.V. Kratz, N. Trautmann, N. Hildebrand, U. Hickmann, C. Frink, N. Greulich  
Mainz University

D.C. Hoffmann, M. Fowler

Los Alamos Scientific Laboratory

H.R. von Gunten

Bern University

The success in synthesizing elements 107<sup>1</sup> and 109<sup>2</sup> at GSI using cold fusion reactions has much revived the interest in the use of the reaction  $^{48}\text{Ca} + ^{248}\text{Cm}$  to make superheavy elements. In addition, recent theoretical calculations describing the limits of fusion gave optimism to predict that  $^{48}\text{Ca} + ^{248}\text{Cm}$  should fuse without significant hindrance, i.e. without "extra-push"<sup>3</sup>. On the other hand, previous experiments to search for superheavy elements by this reaction gave negative results<sup>4</sup>. These experiments were performed approximately 25 MeV above the barrier resulting in excitation energies of the compound nucleus  $^{296}116$  of 40 to 50 MeV. However, the heaviest elements synthesized so far by heavy ion reactions were found to survive at much lower excitation energies of about 20 MeV only<sup>2</sup>.

Based on these new insights into cold fusion reactions we restarted to search again for superheavy elements with  $^{48}\text{Ca}$  plus  $^{248}\text{Cm}$  but at considerably lower excitation energies of the compound nucleus compared to earlier attempts in order to favour low xn-channels.

In a first series of experiments performed in October 82 at LBL off-line chemical techniques were used to search for superheavy elements with half-lives between hours and years. The  $^{48}\text{Ca}$  energy entering 1.7 mg/cm<sup>2</sup> thick  $^{248}\text{Cm}$  oxide targets was 239.0 MeV, i.e. 4 MeV above the calculated fusion barrier of 235 MeV (proximity - 4%<sup>3</sup>). The measured energy spread within the target was 16 MeV(lab) which defines a covered excitation energy range for the compound nucleus  $^{296}116$  of 16 to 29 MeV. Beam integrals accumulated onto the  $^{248}\text{Cm}$  targets were up to  $1.0 \times 10^{17}$  particles. Recoiling reaction products were collected with a copper catcher foil (6.2 mg cm<sup>2</sup>). After each bombardment this foil was chemically processed with similar procedures used already in earlier attempts to search for superheavy elements by heavy ion reactions at the UNILAC<sup>5</sup>. This chemistry is a combination of a gas-phase separation for gaseous and volatile elements and an aqueous procedure aimed to separate bromide complexes from the bulk of reaction products, mainly the actinides<sup>4</sup>. Final samples are presently counted at Mainz University in a low background detection system

which registers single and coincident fission fragments, their kinetic energies and the number of neutrons per fission event.

So far, after a counting time of about 3 months, no fission activity was found in any of the superheavy element samples. The cross section limits for the production of spontaneously-fissioning, long-lived superheavy elements 108 through 116 as it results from all experiments performed are plotted in Fig. 1 (solid-line) as a function of an assumed half-life. The calculated curve is based on a counting period of 3 months, an effective target thickness of  $4.2 \times 10^{18}$   $^{248}\text{Cm}$  atoms, a chemical efficiency for the separation procedure of superheavy elements of 80%, a counting efficiency for fission-fragment coincidences of 60% and an assumed count rate of three events, corresponding to a 95% confidence level if no activity was measured.

1. G. Münzenberg et al., Z. Physik, A300, 107 (1981)
2. G. Münzenberg et al., Z. Physik A309, 89 (1982)
3. W.J. Swiatecki, Nucl. Phys. A376, 275 (1982)
4. see e.g. J.V. Kratz, GSI-82-7 (1982) and Radiochim. Acta, in press
5. H. Gäggeler et al., Phys. Rev. Lett. 45, 1824 (1980)

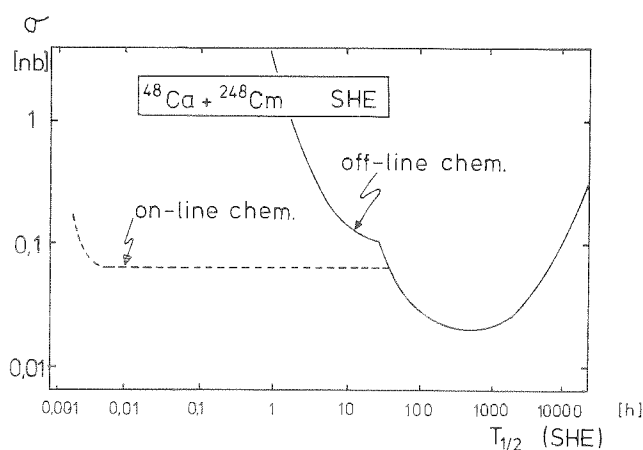


Fig. 1: Cross section limits for the production of spontaneously-fissioning superheavy elements as its results after 3 months counting time (solid-line, for details see text). Also shown is the cross section and half-life range to be covered by a future on-line chemistry experiment (dashed line).



Preparation of Lanthanide and Actinide Samples by Vacuum Evaporation G

C. Frink, N. Trautmann, G. Herrmann  
Institut für Kernchemie, Universität Mainz

M. Schädel  
GSI, Darmstadt

For  $\alpha$ - and spontaneous fission measurements of actinides and superheavy elements carrier free and homogenous sources are needed. Such sources can be prepared by various techniques<sup>1</sup>, most of them are time consuming and, therefore, investigations of short lived nuclides are hampered. For lanthanides and actinides with low evaporation heat samples can be prepared within short times by reduction on a metallic surface with subsequent evaporation and deposition on a cold catcher.

The reducing material must be a thermic stable metal with low adsorption energy such as titanium or zirconium<sup>2</sup>.

In this work experiments with Eu-152, Sm-155 and Am-241 as representatives for lanthanides and actinides were performed in order to determine the optimum evaporation and deposition conditions. The lanthanide activities were produced by neutron irradiations in the Mainz reactor. All the experiments were carried out in a vacuum system as shown in Fig. 1.

In each case 10  $\mu$ l of a nitrate solution was transferred to a titanium crucible and evaporated to dryness converting the nitrate to the oxide. Then the crucible was fixed between two copper holders in the recipient of the vacuum system and the catcher was placed in a distance of some millimeters above the crucible. At a pressure of  $2 \times 10^{-5}$  mbar the crucible was heated by resistance heating for a predetermined time. The temperature of the crucible was measured with a pyrometer. The evaporation and deposition yields were determined after the end of the experiment by  $\gamma$ -spectroscopic measurements of the crucible and the catcher.

The investigated nuclides have been evaporated with a yield of 60-72 % at a temperature of 1000 °C and with 93-95 % at 1070 °C or higher temperatures. The shape of the crucible and the distance between crucible-catcher have great influence on the deposition yields. Crucibles with a large aperture deliver only 20-30 % of the original activity to the collector. If the distance between crucible and catcher is varied from 3 to 10 mm the deposition yield decreases from 85 % (3 mm) to 54 % (10 mm) for Eu-152. This can be explained by the fact that the evaporated activity is not completely collected on an aluminum catcher of 28 mm x 37 mm as shown by autoradiography. At a distance of 3 mm homogenous samples of 12 mm diameter were obtained while at 10 mm the spot smeared out. The evaporation of the investigated nuclides at a temperature of 1070 °C

takes 40-60 s. At higher temperatures (1140 °C) the time is reduced to about 20 s.

The adaption of this technique to a fast automatic high performance liquid chromatography system<sup>3</sup> requires a cylindrical crucible with a hole of 6 mm and a volume of about 1 ml. Evaporation rates of  $\sim 85$  % (1150 °C) and deposition yields of  $\sim 70$  % were obtained with this type of crucible at a crucible-catcher distance of 4 mm and an evaporation time of 60-80 s.

The good quality of the samples obtained with this method was checked with Am-241 samples and  $\alpha$ -spectrometric measurements with a surface barrier detector yielding a FWHM of 32 keV compared to a FWHM of 37 keV achieved with samples prepared by molecular plating.

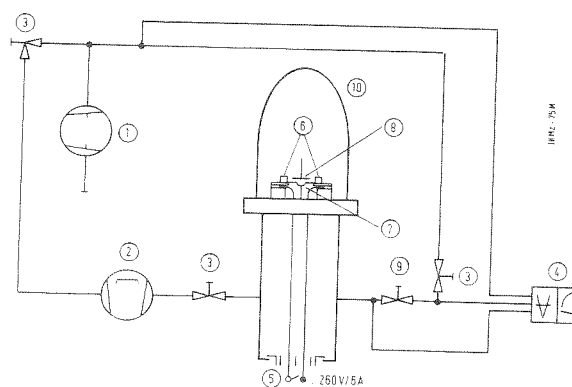


Fig. 1: Schematic diagram of the evaporation system  
① ② pumps; ③ ⑨ valves; ④ vacuummeter; ⑤ ⑥ resistance heating; ⑦ crucible; ⑧ catcher; ⑩ quartz bell

- 1 W. van der Eijk et al, Nucl. Instr. Meth. 112, 343 (1978)
- 2 E. Rhede et al., Zentralinstitut für Kernforschung Rossendorf ZfK 367 (1978) S. 23
- 3 W. Schorstein et al. GSI Scientific Report 82-1, 220 (1981)

Chemical Separation of Thorium, Protactinium, Uranium, Neptunium and Plutonium  
from Complex Heavy Ion Reaction Product Mixtures <sup>G</sup>

M. Lerch, U. de la Chevallerie, D. Gembalies-Datz, W. Kieling, J.-V. Kratz,  
 A. Lewening, N. Trautmann, S. Zauner, G. Herrmann

Institut für Kernchemie, Universität Mainz

A method for the separation of Th, Pa, U, Np and Pu from heavy ion reaction product mixtures was developed for i) the measurement of cross-sections for sub-Coulomb transfer in collisions of  $^{238}\text{U}$  with  $^{238}\text{U}$  and ii) the radiochemical determination of actinide cross-sections in the  $^{48}\text{Ca}+^{248}\text{Cm}$  reaction. The separation is based on differences in the ion exchange behaviour of these elements from hydrochloric and nitric acid solutions.

Pa, U, Np and Pu form strong chloro-complexes which can be adsorbed from 8 N HCl on an anion exchange column whereas Th and the transplutonium elements (TPE) pass through. Th is adsorbed from 8 N  $\text{HNO}_3$  on a second anion exchange column while the transplutonium elements are not retained. Desorbents for the subsequent elution of Th, Pa, U, Np and Pu are summarized in Table 1.

Table 1

Separation of Th, Pa, U, Np and Pu on anion exchange columns (BioRad AG 1x8, -400 mesh)

	element	desorption with
1st anion exchange column; adsorption from 8 N HCl	Th + TPE	8 N HCl
	Pa	8 N HCl/0.05 N HF
	Pu	8 N HCl/ $\text{NH}_2\text{OH}\cdot\text{HCl}/\text{NH}_4\text{I}$
	Np	4 N HCl/0.05 N HF
	U	0.5 N HCl
2nd anion exchange column; adsorption from 8 N $\text{HNO}_3$	TPE	8 N $\text{HNO}_3$
	Th	2 N HCl <sup>3</sup>

In the  $^{238}\text{U}+^{238}\text{U}$  experiments<sup>1</sup>, targets and recoil product catchers were processed separately, since the initial dissolution steps are different for the uranium targets and the gold catcher foils.

The uranium targets on titanium backings were dissolved in hot 10 N HCl/0.01 N HF. With  $\text{H}_3\text{BO}_3$  the fluoride complexes were destroyed and with a few drops of conc.  $\text{HNO}_3$ , Pu(III) was oxidized to Pu(IV) before column injection. The gold catcher foils after segmentation into bins of laboratory angles were dissolved in aqua regia and Au was removed by extraction with diethyl ether. After evaporation and dissolution in 8 N HCl, the aqueous phase was submitted to column separation.

Counting sources of Pa and Np for  $\gamma$ -spectroscopic measurements were prepared by coprecipitation of these elements with  $\text{Fe}(\text{OH})_3$ . U from the target processing was precipitated as  $(\text{NH}_4)_2\text{U}_2\text{O}_7$ . Th, Pu and U from the catcher treatment were electrodeposited on tantalum foils for  $\alpha$ -particle spectroscopy. Before electrolysis traces of

iodine had to be removed from the plutonium fraction. Therefore, Pu was coprecipitated with  $\text{Zr}(\text{OH})_4$ , the precipitate dissolved in 0.5 N HCl/0.025 N HF and, after reduction of Pu with  $\text{NH}_2\text{OH}\cdot\text{HCl}$ , transferred to a small cation exchange column. The fluoro-complex of Zr passed through while Pu was adsorbed and could be eluted with 4 N HCl.

For the measurement of cross-sections for relatively short-lived transfer products (e.g. 37 min  $^{236}\text{Th}$ , 8.7 min  $^{237}\text{Pa}$  etc.) in the  $^{238}\text{U}+^{238}\text{U}$  system<sup>1</sup> chemical separations and the preparation of suitable counting samples had to be accomplished rapidly. Separate processing of the targets and the catcher foils - in these experiments Cu was used as catcher material - was necessary.

The targets were dissolved in a HCl/HF mixture. The copper catcher foils were dissolved in a hot mixture of conc. HCl and  $\text{HNO}_3$  (3:8) and the actinides were coprecipitated with  $\text{La}(\text{OH})_3$  using ammonia. In this step Cu was removed as the diamine complex. Pa was isolated from the feed solutions resulting from the dissolution of the targets and the  $\text{La}(\text{OH})_3$  precipitate by extraction chromatography with di-isobutylcarbinol (DIBC). Then Th and U were separated by ion exchange (see Tab.1).

Sources for  $\gamma$ -ray spectroscopy were prepared by coprecipitation of Th, Pa and U with  $\text{Fe}(\text{OH})_3$ . In the target processing U was precipitated as  $(\text{NH}_4)_2\text{U}_2\text{O}_7$ .

In the  $^{48}\text{Ca}+^{248}\text{Cm}$  experiment<sup>2</sup> the reaction products were stopped in a copper catcher foil. After removal of volatile elements by a gas-phase chemistry the catcher was dissolved in dilute HBr and this solution passed through a cation exchange column. With 0.1 N and 0.8 N HBr the SHE fraction was eluted. Then U and Cu were eluted with 2.5 N HCl containing a few drops of bromine, the actinides were desorbed with 6 N HCl, and finally Th with oxalic acid. The actinide and the U/Cu fractions - after removal of Cu as the diamine complex in a  $\text{La}(\text{OH})_3$  precipitation step - were treated as described in Table 1. The thorium fraction after conversion to the nitrate system was injected onto an anion exchange column.

Th, Pa and U were electrodeposited directly from the effluents of the anion exchange columns. The plutonium fraction had to be purified prior to electrolysis as described before.

<sup>1</sup> G. Wirth et al., this report

<sup>2</sup> H. Gäggele et al., this report

Rapid Preparation and Gaschromatographic Separation of Carrier-Free  
Lanthanide Hexafluoroacetylacetonates <sup>G</sup>

N. Greulich, N. Trautmann, G. Herrmann  
Institut für Kernchemie, Universität Mainz

The investigation of neutron-rich or neutron-deficient actinide nuclides produced in heavy-ion reactions requires fast procedures for their isolation. For unravelling actinide or lanthanide mixtures, multistep processes have to be applied. Gaschromatography is one powerful tool for the fast separation of small quantities, because the mobile phase can be operated with a high flow-rate without losses in separation efficiency. A prerequisite for rapid performance is the fast preparation or formation of volatile compounds with subsequent separation in a gaschromatograph. Due to their similar chemical properties homologous lanthanide elements can be used to study the applicability of gaschromatographic methods for the isolation of actinides.

Carrier-free lanthanide isotopes were produced by neutron induced fission of  $^{235}\text{U}$  and were transported continuously with a  $\text{KCl}/\text{N}_2$ -gasjet out of the target chamber. The  $\text{KCl}$ -clusters, together with the attached fission-products, were trapped in two glass-fiber filters. After 30 min of irradiation time, they were dissolved in an aqueous solution of  $\text{NaH}_2\text{PO}_2$ . A reducing agent is required for quantitative extraction of lanthanides at moderate pH-values. The lanthanides, together with some other fission products, are extracted within 10 s with a mixture of 0.05 M hexafluoroacetylacetonone (HHFA) / 0.035 M tri-n-butylphosphate (TBP) in cyclohexane<sup>1</sup>. The distribution coefficients for some lanthanides and other fission products from various aqueous phases into a 0.05 M HHFA / 0.035 M TBP cyclohexane solution are given in table 1. Obviously, a reducing aqueous medium gives the best extraction yields for yttrium and the lanthanides and the lowest values for undesired accompanying fission products.

For the gaschromatographic separation of yttrium and the lanthanides, 0.1 ml of the organic phase is syringed into the injector of a gaschromatograph<sup>2</sup>. With a carrier-gas (70 ml/min  $\text{N}_2$ ) loaded with HHFA passing the  $\text{N}_2$  through HHFA at 40°C, a decomposition of the  $\beta$ -diketonates in the column (2 m long, glass, 2.4 mm inner diameter, 1% PPE 20 on Chromosorb G 80-100 mesh) is prevented. The injection temperature was kept at 250°C, the column temperature was increased from 150°C to 250°C with a rate of 10 °C/min. Fig. 1 shows a chromatogram obtained under these conditions, together with the temperature gradient. Iodine, which is partly extracted, appears first in the eluate, then yttrium followed by the individual lanthanides according to their decreasing ionic radii of the threevalent states. The gap between yttrium

and the lighter lanthanides can be explained by its relatively large radius of 0.89 Å which corresponds to that of  $\text{Ho}^{3+}$ . Total retention times between 3.5 (Y) and 12.5 min (La) were measured. The alkaline earth elements also extracted into the organic phase (see table 1) are not volatilized. The described method should also allow the separation of individual actinide elements within a few minutes.

<sup>1</sup> W.C. Butts and C.V. Banks, Anal. Chem. **42**, 133 (1970)

<sup>2</sup> N. Greulich, N. Trautmann and G. Herrmann, GSI Scientific Report **82-1**, 219 (1981)

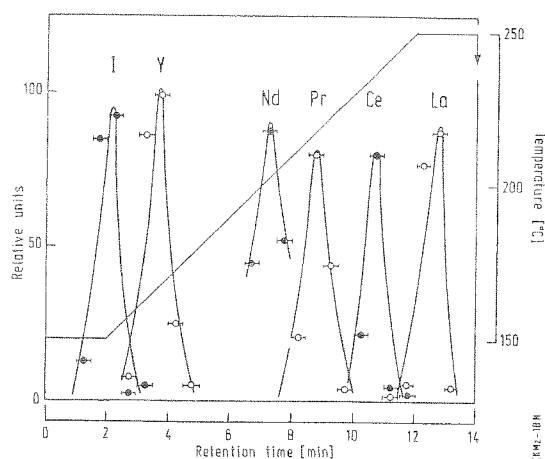


Fig. 1 Separation of lanthanide hexafluoroacetylacetonates by temperature-programmed gaschromatography

Table 1

Distribution coefficients for the extraction of lanthanides and some other fission products from various aqueous phases with 0.05 M HHFA/0.035 M TBP in cyclohexane

Element	aqueous phase		
	0.3 m $\text{Na}_2\text{PO}_2$	$\text{H}_2\text{O}$	0.3 m $\text{H}_2\text{O}_2$
Y	141	74	1.9
La	$\infty$	52	1.1
Ce	41	66	3.5
Pr	68	75	2.0
Nd	$\infty$	$\infty$	2.1
Mo	$3 \cdot 10^{-3}$	$3 \cdot 10^{-3}$	0
Tc	0	$4 \cdot 10^{-3}$	0
Rb	0	0.012	-
Cs	0	0.011	0.03
Sr	1.47	1.73	1.39
Ba	1.32	1.10	1.25
Te	0.38	0.52	0.49
I	0.72	0.91	0.57

0 = not detectable in the organic phase

$\infty$  = not detectable in the aqueous phase

M. Brügger, Th. Karlewski, N. Trautmann  
 Institut für Kernchemie, Universität Mainz  
 A.K. Mazumdar, H. Wagner, W. Walcher  
 FB Physik, Philipps-Universität Marburg

For studies on short lived lanthanide nuclides the heliumjet on-line isotope separator HELIOS<sup>1</sup> has been equipped with a fast tape transport system. This tape transport system consists of a high vacuum chamber, diffusion slits and the drive electronics. The vacuum of  $1 \times 10^{-5}$  mbar in the separator beamline as well as in the high vacuum chamber is obtained by means of a 3000 l/s diffusion pump. By differential pumping through the diffusion slits the atmospheric pressure is reduced stepwise. The mass separated ion beam is implanted into the transport tape (computer tape) at an energy of 20 keV. After collecting the activity it is transported through the diffusion slits to the detector station, where  $\gamma$ -singles,  $\gamma, \gamma, t$ -coincidence and  $\gamma, \gamma, t$ -angular correlation measurements can be performed. The tape is driven by a stepping motor and the velocity is controlled by a microprocessor system. The maximum speed of the tape is 10 m/s in the continuous mode and 6 m/s in a start-stop mode obtaining a stopping accuracy of  $\pm 1$  mm. With this tape unit  $\gamma$ -singles,  $\gamma, \gamma, t$ -coincidence and  $\gamma, \gamma, t$ -angular correlation measurements on 2.3 min  $^{148}\text{Pr}$  and 6.2 s  $^{150}\text{Pr}$  were performed using a  $6.5 \text{ mg/cm}^2$   $^{235}\text{U}$  target in the gasjet system and the high temperature surface ionization source<sup>2</sup>. Several new  $\gamma$ -lines could be assigned to the decay of these transitional nuclides and partial decay schemes were established.

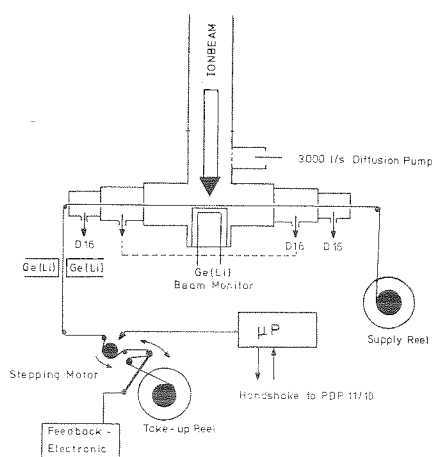


Fig. 1: Schematic drawing of the HELIOS tape system

Furthermore, the optimal operating conditions for the integrated plasma ion source of the HELIOS system<sup>3</sup> with respect to the ionization of light fission products (mass number 83 - 85) were explored. Since the fission yields for arsenic and selenium in the mass region 83 -

85 are rather low the optimization experiments were performed with their homologues, for which the efficiency measurements of the He/KCl-jet plasma ion source have already been made<sup>4</sup>. In Table 1 efficiency values of antimony and tellurium isotopes yielding from measurements behind the ion source with two different cluster materials are summarized. With  $\text{PbCl}_2$  an enhancement by a factor of 2 compared to KCl could be observed<sup>2</sup>.

Table 1

Efficiency values for the HELIOS system using two different cluster materials

Nuclide	Efficiency/%	Clustermaterial
$^{131}\text{Sb}$	0.82	$\text{PbCl}_2$
	0.46	KCl
$^{133}\text{Te}$	0.46	$\text{PbCl}_2$
	0.27	KCl
$^{134}\text{Te}$	1.06	$\text{PbCl}_2$
	0.60	KCl

In Table 2 the overall efficiency values of the HELIOS system for  $^{84}\text{As}$ ,  $^{84}\text{Se}$  and  $^{85}\text{Se}$  under optimum conditions using  $\text{PbCl}_2$  as cluster material in the gasjet are given.

Table 2

Overall efficiency values for the HELIOS system

Nuclide	Efficiency / %
$^{84}\text{As}$	$0.5 \times 10^{-2}$
$^{84}\text{Se}$	$1.0 \times 10^{-2}$
$^{85}\text{Se}$	$1.5 \times 10^{-2}$

1/ A.K. Mazumdar et al., Nucl. Instr. and Meth., **174** 183 (1980)

2/ M. Brügger et al., GSI Scientific Report 1981, **82-1**, p. 225

3/ A.K. Mazumdar et al., Nucl. Instr. and Meth., **139** 319 (1976)

4/ W. Ziegert et al., Jahresbericht, Inst. f. Kernchemie Mainz, 1980, p. 22

Solar Cells as Detectors for Fragments of Volatile Spontaneously Fissioning Nuclides G

N. Hildebrand, W. Kieling, N. Trautmann, G. Herrmann  
Institut für Kernchemie, Universität Mainz

M. Brügger, H. Gäggeler, K. Sümmerer, W. Weber  
GSI, Darmstadt

In the search for superheavy elements detection of spontaneous fission activity provides the most sensitive method. From the predicted chemical and physical properties some superheavy elements such as 112 and 114 are expected to be volatile at room temperature. So far such species could be measured only in  $2\pi$ -geometry by a surface barrier detector (ring detector) through which the gases were transported and condensed on a cooled copper-surface placed opposite to the detector. By the application of thin photovoltaic cells, cooled from the backside by a cryogenic pump and acting both as a condensing surface (down to 70 K) and as a fission fragment detector<sup>1</sup> it is possible to perform  $4\pi$ -measurements under coincidence conditions. The energy resolution for fission fragments of monocrystalline as well as polycrystalline solar cells from different suppliers was determined with a  $^{248}\text{Cm}$ -source using conventional electronics and applying no bias voltage. The best results with respect to temperature and energy resolution were obtained with a monocrystalline cell from AEG with 100  $\mu\text{m}$  thickness and  $\approx 200 \text{ mm}^2$  active surface. Fig. 1 shows the energy spectrum of  $^{248}\text{Cm}$ -fission fragments obtained with such a photovoltaic cell demonstrating a peak-to-valley ratio of 2:1.

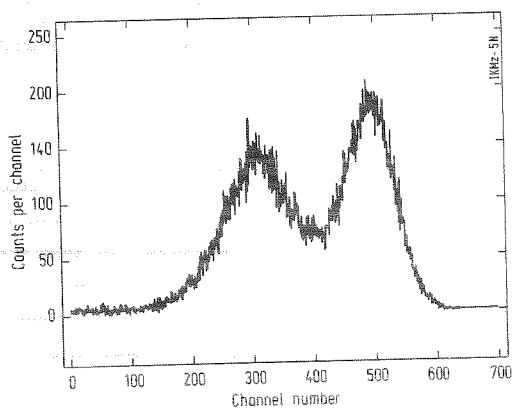


Fig. 1: Energy spectrum of  $^{248}\text{Cm}$  fission fragments measured with a solar cell

Furthermore coincidence measurements were made with the solar cell and a surface barrier detector (ring detector) to define the optimal coincidence conditions. The tests with a  $^{248}\text{Cm}$  source on a thin carbon foil demonstrated that the total kinetic energy of the fission fragments can be determined with a FWHM of 23 MeV.

In the next step the solar cell was fixed to the cold head of a cryo pump and the energy spectrum was measured

at 70 K. No drastic decrease in the energy resolution was observed. In the set-up modelling the final experimental conditions, an annular surface barrier detector was positioned opposite to the solar cell in the cryogenic chamber (Fig. 2). A capillary through which

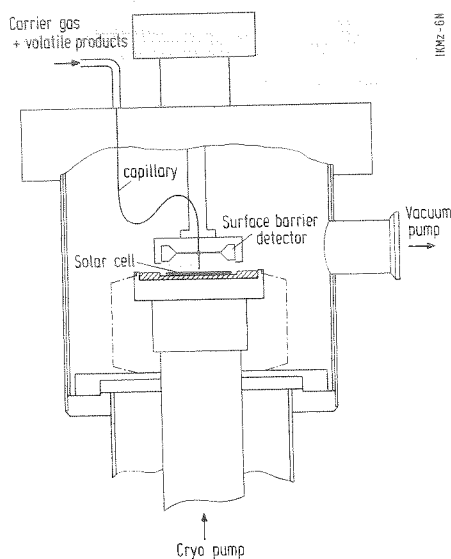


Fig. 2: Schematic diagram of the cryogenic chamber with an annular surface barrier detector and a solar cell for measurement of volatile spontaneously fissioning nuclides under  $4\pi$  geometry and coincidence conditions.

the volatile products are transported by means of a carrier gas (argon) is passed through the hole of the surface barrier detector ending 1 mm above the solar cell. This arrangement allows to measure  $E_1/E_2$  coincidences from gaseous spontaneously fissioning nuclides.

The condensation efficiency of the set-up was investigated with radon isotopes (4.0-s  $^{219}\text{Rn}$ , 56-s  $^{220}\text{Rn}$ , 3.8-d  $^{222}\text{Rn}$ ) liberated from  $^{227}\text{Ac}$ -,  $^{228}\text{Th}$ - and  $^{226}\text{Ra}$ -sources and transported with argon as carrier gas through the capillary. A temperature of 70 K on the cold head of the cryo pump can be maintained for a carrier gas flow rate of up to 150 ml/min. The condensation yield for radon was determined by  $\alpha$ -spectroscopy with the ring detector. The cryogenic chamber with the solar cell was for the first time applied in a search for gaseous superheavy elements in the  $^{48}\text{Ca}+^{248}\text{Cm}$  experiment<sup>2</sup> performed in October 1982.

<sup>1</sup> G. Siebert, Nucl. Instr. Meth. 164, 437 (1979)

<sup>2</sup> H. Gäggeler et al, this report, p.